AD-A122 228 EFFECTS OF MASS TRANSFER ON TRANSITION BEHAVIOR AT HIGH SPEEDS..(U) POLYTECHNIC INST OF NEW YORK BROOKLYN DEPT OF MECHANICAL AND A.. P PLOSTINS ET AL. JUN 82 1/1

UNCLASSIFIED POLY-M/AE-829 AFOSR-TR-82-1030 F/G 16/3 NL

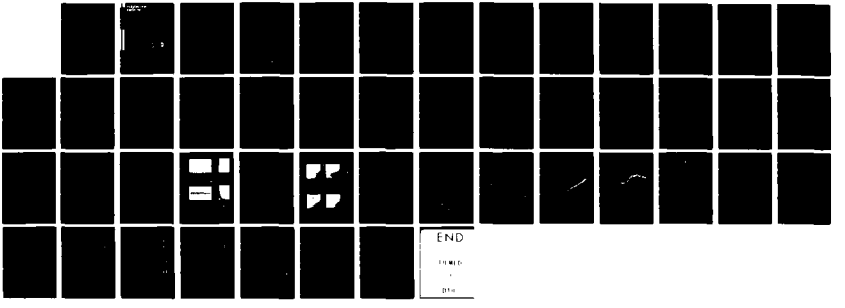

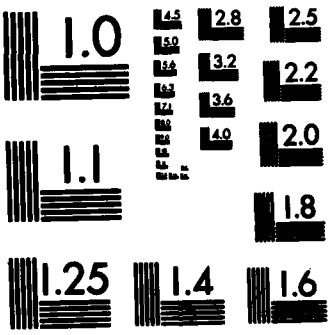

Polytechnic Institute of New York

AFOSR-TR- 82-1030

12

EFFECTS OF MASS TRANSFER ON TRANSITION BEHAVIOR AT HIGH SPEEDS

By P. Plostins and R. J. Cresci

June 1982

Contract No. AFOSR 81-0018

POLY-M/AE ~~Report No.~~ 82-9

Approved for public release;
distribution unlimited.

EFFECTS OF MASS TRANSFER ON TRANSITION BEHAVIOR AT HIGH SPEEDS

Peter Plostins and Robert J. Cresci
Polytechnic Institute of New York
Farmingdale, New York

M sub infinity

ABSTRACT

Surface heat transfer and boundary layer transition measurements have been performed on a slender blunted cone at $M_\infty = 8.0$. These measurements have been obtained on the conical surface with mass transfer occurring on the spherical nose cap. The free stream Reynolds number, based on nose radius, varied between ~~0.6×10^4~~ and ~~0.9×10^5~~. Data was obtained both at zero angle of attack and at angles as high as ~~14°~~, which exceeds the semi-vertex cone angle of ~~10°~~. The technique utilized in the determination of transition location was the observation of the RMS output of a thin film gauge, imbedded in the model surface, and maintained at a constant temperature by an anemometer system. A sudden change in the RMS output of the film gauge was found to accurately locate the onset of boundary layer transition.

Table of Contents

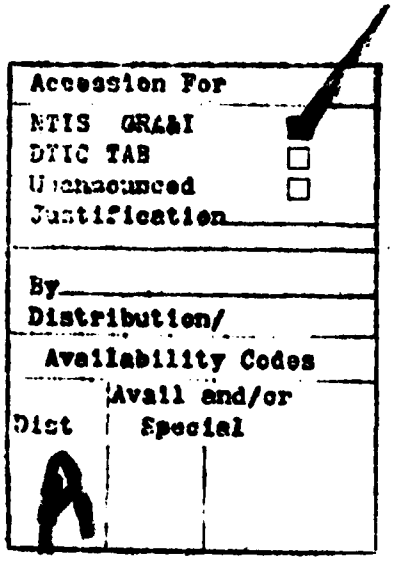

List of Symbols

A	Area ($ft.^2$)
C_p	Specific Heat at Constant Pressure (BTU/lb°R)
H	Stagnation Enthalphy (BTU/lb)
m	Mass Flux (slugs/sec)
N_c	Injection Similarity Parameter
Nu	Nusselt Number
P	Pressure (lbs/ft^2)
Pr	Prandtl Number
$\dot{q}$	Heat Transfer Rate (BTU/sec)
R_o	Nose Radius (ft)
Re_∞	$(\frac{\rho_\infty V_\infty R_o}{\mu_\infty})$ Free Stream Reynolds Number
Re_θ	$(\frac{\rho_e u_e \theta}{\mu_e})$ Reynolds Number Based on Momentum Thickness
r	Axisymmetric Radius (ft)
s	Downstream Coordinate (ft)
T	Temperature (°R)
t	Time (sec)
u	Streamwise Velocity Component (ft/sec)
V_∞	Freestream Velocity (ft/sec)

Greek Symbols

α	Angle of Attack (deg)
β	Velocity Gradient (du/ds) (1/sec)
Δ	Local Model Wall Thickness (ft)
γ	Ratio of Specific Heats
μ	Viscosity Coefficient ($lb\text{-}sec/ft^2$)
θ	Momentum Thickness $\theta = \int_0^\infty \rho u (u_e - u)\, dy$
ϕ	Transverse Coordinate (deg)
ρ	density ($slugs/ft^3$)

Subscripts

c	coolant
e	Boundary Layer Edge Condition
i	At the End of the Injection Region

se	Boundary Layer Edge Condition in the Stagnation Region
t	Stagnation Conditions (Venturi)
tr	Transitional
w	Wall Value
2	At the Venturi Throat

Superscripts

-	Non-Dimensional Quantity
∿	Lees Transformed Variable

List of Figures

EFFECTS OF MASS TRANSFER ON TRANSITION BEHAVIOR AT HIGH SPEEDS

by

P. Plostins and R. J. Cresci

I. Introduction

Mass transfer has been known to provide a significant cooling effect in high speed laminar boundary layers. In recent years, this basic concept has been proposed for alleviation of heating problems of re-entry vehicles, including the space shuttle, cf. ref. (1). Planetary probes designed for entry into the atmosphere are also associated with large mass transfer rates in the stagnation region, ref. (2)-(4). Here, the mass transfer results from the large radiative heat transfer occurring in the stagnation region; this results in large ablation rates which produce "massive blowing". For these large injection rates, a layer of injected gas occurs adjacent to the surface which is essentially at the surface temperature. This insulating layer prevents any convective heating at the surface. A numerical treatment of this problem was first obtained in reference (5) where the constant property layer was seen to thicken rapidly with mass transfer rate and the high shear layer was displaced outward from the surface. These effects were verified experimentally in reference (6) where the alteration of the inviscid flow field was observed by schlieren photographs and downstream effects of the mass transfer were also studied.

On a slender body, whether mass is injected by an active coolant system or whether the injection occurs as a result of surface ablation, the major transfer of mass will occur in the stagnation region followed by a surface on which the effective injection rate is zero (or extremely small). In the ablation system, this is

caused by the radiation from the high temperature gases behind the bow shock wave in the nose-cap region. As the shock weakens in the downstream direction and becomes more conical in shape, the gas temperature drops rapidly and, along with it, the attendant surface ablation. If one considers the active coolant system, again one finds that the surface mass transfer is confined to the stagnation region since in this case the minimum injection required for reduction of convective heating is the important consideration. In either situation, however, there will be some residual cooling effect as the injected fluid flows downstream within the boundary layer.

It has been observed in ref. (6) that this increased boundary layer mass flow will initiate transition to turbulence earlier than in a boundary layer with no upstream injection. Although small amounts of film cooling have been known to decrease the surface heat transfer rate, if the free stream Reynolds number is sufficiently large, the injected fluid may initiate transition which would not normally occur. In a transitional or turbulent boundary layer, the local heat transfer is usually significantly higher than that in a laminar flow at the same free stream conditions. As a result, it is extremely important to be able to determine the onset of transition when such active cooling systems are proposed, or when they occur naturally through surface ablation. In either condition, one may be trading a lower heating rate in the stagnation region for a higher rate downstream. Since the downstream area can be significantly larger than the surface area in the stagnation region, the total heat absorbed by the vehicle may actually be greater with massive blowing than without under certain conditions.

Since transition for specific configurations can only be obtained experimentally, there is relatively little information available in the open literature on this subject. Reference (7) provides experimental data on a porous hemisphere within one nose radius of the stagnation point of a spherically blunted cone which indicates the effects of increasing mass injection rate on the onset of transition. In fact, transition was observed in this paper even at the stagnation point itself for sufficiently large values of the mass transfer rate. In reference (8) velocity profiles and boundary layer thicknesses were measured on a blunted cone by pitot probes and a hot wire anemometer. Transition was observed on the spherical nose in this case at relatively low values of the injection rate. A NASA study, ref. (9), of blunt bodies with distributed injection also found transitional effects as a function of the mass injected in the boundary layer at various Reynolds numbers from the surface heat transfer measurements. In reference (10) similar effects were obtained from surface shape distributions of ablating graphite nosetips in hypersonic flight. Downstream effects of mass injection on a slender cone were obtained in reference (11) from surface heat transfer measurements; these measurements were then used to attempt to correlate the transition location with mass transfer rate and free stream Reynolds numbers. This is the only previous study, to the authors' knowledge, of transition located on the impermeable surface downstream of the mass transfer region. One of the more surprising results that was obtained from ref. (11) was that transitional flow was observed close to the injection region, followed by a region of laminar flow which in turn was followed by another region of transitional and

ultimately turbulent boundary layer. This behavior occurred only at certain Reynolds numbers and implied a local relaminarization of the boundary layer. In order to interpret these results, the numerical analysis of reference (12) was modified in reference (11) to account for mass transfer in the stagnation region. This analysis was then utilized to predict the boundary layer characteristics under the test conditions. In the past, a parameter which has been used quite successfully to correlate the onset of transition is the local Reynolds number based on momentum thickness. When this was computed from the numerical analysis, it was observed to decrease along the surface and subsequently increase in the downstream direction under certain combinations of mass flow rate and Reynolds number. A direct correlation of this parameter as computed from the numerical analysis was then applied to the experimental results. Although this correlation appeared to provide an explanation of the anomolous behavior observed, the method of transition detection, i.e., measurement of the surface heat transfer rates, was not felt to be extremely accurate.

The purpose of the present study was to attempt to measure the onset of transition, on the impermeable surface, with greater accuracy than is possible by interpretation of surface heat transfer measurements. This was accomplished by using thin surface films which were heated and monitored by a constant temperature hot wire anemometer system. This technique, described in the following sections, was used to accurately locate the transition point under a variety of free stream Reynolds numbers, surface locations, and mass injection rates. The study was performed at a free stream Mach number of 8.0 on a spherically blunted cone of

10° half angle. Although the major portion of this study was conducted at zero angle of attack, some tests were run at angles of attack between 2° and 14°. Both the downstream effectiveness and the transition location were also measured under these flow conditions.

II. Instrumentation and Experimental Procedures

The test program was conducted in the hypersonic facility of the Polytechnic Institute of New York. The tests were performed in a Mach 8.0 blow down wind tunnel, which has a two foot diameter, axisymmetric test section. The freestream stagnation temperature of the flow was maintained at 2000°R.; this is accomplished by heating the air in a pebble bed heater. The stagnation pressure of the air in the heater may be varied from 50 to 600 psia. The above stagnation conditions correspond to a range of freestream Reynolds numbers of 1.13×10^4 to 1.35×10^5 per inch. The average test duration was on the order of ten seconds. A sting located in the tunnel behind the test section is capable of positioning a model at angles of attack over a range of $\pm 14°$ in 2° increments.

A sketch of the primary model used in the current test program is shown in figure (1). It consists of a 10° half angle cone with a spherical nose cap of 1.1 inch radius. The porous injection region extends over a total included angle of 60°. For measurements in the vicinity of the injection region, this model was used; for downstream data, another model was used which was geometrically similar but with a nose radius of 0.5 inches. The larger dimensions of the model shown in figure (1) facilitated installation of the instrumentation in the nose region. A porous plug machined out of

a flat sheet of sintered stainless steel powder subtends a total spherical angle of 60° at the nose of each model. This porous plug is removable and can be replaced with a thin walled stainless steel cap for zero injection tests. Behind the porous plug each model is fitted with a coolant settling chamber. During a test the pressure and temperature of the coolant in the settling chamber were recorded.

Although surface heat transfer measurements were obtained in the current test program, the primary objective was to develop a technique which more accurately ascertained the transition location on the model. In the past, various methods have been utilized in the determination of transition location, e.g., surface heat transfer, Preston tubes, and thin film gauges. In the current test program it was decided to use the thin surface film technique. The gauges utilized are the standard TSI miniature flush mounted sensors in which the film is deposited on the end of a quartz cylinder 1.5mm in diameter. The cylinder is mounted in a hole drilled in the model so that the cylinder end is flush with the model surface. The film gauge is held in place by epoxy and due to the relatively large model radius of curvature, presents an essentially smooth continuous surface. The gauge is maintained at a temperature slightly higher than that of the surrounding model by a Thermosystems Series 1050 constant temperature anemometer which is used to power the gauges and obtain the sensor output. The root mean square characteristics of the output signals from the sensor elements are analyzed by a Thermosystems Model 1076 true root-mean-square meter. During a typical test the time constant on the meter was maintained at 1/10 of a second.

Validyne AP10 absolute pressure transducers were used to monitor the pertinent pressure data such as coolant chamber pressure, freestream stagnation pressure and freestream static pressure.

The output of the anemometer, the RMS meter, the thermocouples and the pressure transducers was fed into a bank of Honeywell Accudata 122 linear amplifiers. The amplifiers normalized all incoming signals to a range of 0.0 to 1.0 volts. This normalized output was recorded on a Honeywell Model 101 AM-FM magnetic tape recorder. The tape recorder is capable of recording 28 channels of data in an FM mode up to a frequency of 5KHz. In the AM mode AC signals up to 600 KHz can be recorded. The microprocessor of the Model 101 can mark each channel with a timing pulse so that all recorded data may be correlated in real time.

After the wind tunnel test run is terminated, the data recorded on the tape recorder is played back into a Digital PDP11-34 computer which has an AR-11 laboratory peripheral system. The AR-11 system is capable of analog to digital conversion of 16 channels of analog data. The digitized data is stored by the PDP11-34 on a diskette and is then ready for processing and analysis.

III. Transition Detection Technique

Since the main objective of this study was to obtain accurate transition locations for various mass injection rates, the techniques used for this determination were reviewed. In reference (10) transition was determined by the observation of ablated nose shapes; transitional and turbulent heat transfer were found to produce a distinct difference in the resulting shape as well as a distinguishable macroroughness surface pattern. References (6) and (11) util-

ize the measurement of surface heat transfer rates either under varying Reynolds number or varying mass injection conditions. This provides a reasonable indication of transitional behavior but does not locate the exact initiation point. Preston tubes have been used in references (13) and (14) and rely on the abrupt alteration of velocity profile in the boundary layer which is produced in a transitional flow. Although this is a good technique for boundary layers without injection, it was not clear how the velocity profiles would behave at transition since they have already been altered to some degree by mass transfer effects.

Reference (15) utilized thin surface films to measure the unsteadiness that occurs in the boundary layer under transitional conditions. It was also found to accurately indicate the exact location of transition initiation, and therefore, was the approach used in the current study.

In order to examine the characteristic behavior of these gauges, one was installed on the inner surface of a tube and various flow rates were then established to produce a laminar, transitional, and subsequently turbulent flow in the pipe, at low subsonic velocities. The output signals of the TSI constant temperature anemometer are shown in figure (2), and for Reynolds numbers based cn pipe diameter of 452 and 8480, the typical laminar and turbulent behavior is evident. The signal was also recorded on a high speed magnetic tape system and was then fed into a spectrum analyzer; the spectral distributions are included in figure (2) for the same flow conditions. The initial spike observed in the spectrum, at zero frequency, is characteristic of the analyzer and is used for amplitude calibration; it is not indicative of the

signal amplitude at low frequency. It may be observed that transition onset under these conditions is evident from both the raw signal data and the spectral distribution.

This technique is seen to work quite well for subsonic flows; however, when subsequently tried in the hypersonic wind tunnel facility, the tunnel noise obscured the exact definition of the transition location as observed from the spectrum analysis. The surface heat transfer data at a distance 47.0 nose radii downstream of the stagnation point as measured on the conical model at Mach 8.0 are shown in figure (3) versus coolant flow rate. With zero injection, the flow is clearly laminar and transition is seen to occur at coolant flow rates in the vicinity of $.6 \times 10^{-4}$ slugs/sec. If one examines the spectral distribution of the hot film output signal (cf. fig. (4)), it is difficult to evaluate where transition occurs due to the background tunnel noise. Even for zero coolant flow, where the boundary layer is clearly laminar, the anemometer signal shows a significant spectral distribution. This is typical of the data obtained under all test conditions, in the Mach 8 hypersonic tunnel.

Another approach investigated was to examine the RMS voltage for various tests, rather than the spectral distribution of the fluctuating signal. The advantage of using the RMS voltage can be clearly seen from Fig. (3). In Fig. (3) it is obvious that the RMS voltage defines the transition location at least as sharply as the surface heat transfer data, and significantly better than the spectral distribution.

At large downstream locations, where transition occurs rapidly, the surface heat transfer measurements were found to provide a

reasonably accurate indication of transition location. However, closer to the injection region where transition is spread out over a larger distance, the heat transfer does not indicate a distinct jump from laminar flow conditions. Figure (5) shows the typical surface heat transfer behavior at a location 2.95 nose radii from the stagnation point. Also included is the numerical analysis of reference (11) for a purely laminar boundary layer. Comparison of the heat transfer data with the analysis indicates a deviation which could be caused by transition, however, since the data is still decreasing monotonically with increasing mass transfer, it is very difficult to establish an exact location for transition. Examination of the RMS data from the thin film, on the other hand, does accurately define the transition location ($m_{c_{tr}} \simeq .8x10^{-4}$) without having to rely on the accuracy of a numerical analysis of the boundary layer.

The only difficulty associated with this technique is that a large number of tests were required to locate the transition point, i.e., each data point in figure (5) corresponds to a different test run. With the high speed tape data acquisition system described in the previous section, it was decided to run a variable mass injection test at a constant Reynolds number to evaluate the possibility of obtaining the transition location in one test run. Figures (6) and (7) show the results of these tests. Figure (6) presents the coolant chamber pressure vs. time and the RMS signal vs. time at a surface location of $\bar{s} = 36.8$ and a free stream Reynolds number of $4.0x10^4$. The location of transition is clearly evident on the RMS plot and determines the injected mass transfer rate required to initiate transition. The same information is shown in figure (7) for

a Reynolds number of 5.1×10^4, a location of 9.09 nose radii downstream of the stagnation point, and an angle of attack equal to 2 degrees. From these tests, an accurate determination of the initiation of transition can be observed in terms of the mass flow rate, at a given surface location. All the subsequent information, on boundary layer transition, described in this paper was obtained by utilizing this technique.

Clearly, the RMS output of the surface film gauges may be used to determine transitional behavior even when active cooling is present. They provide a means for determining the transition location without resorting to a theoretical analysis of the flow field. Moreover, configurations and flow fields may be investigated for which no theoretical analysis is presently available, e.g., angle of attack conditions.

IV. Presentation and Discussion of Results

To establish the rate of coolant flow at any time during a test a venturi with a contraction ratio of one hundred to one was installed in the coolant supply line. Throughout the test the upstream pressure, P_t, stagnation temperature, T_t, and throat pressure, P_2, are recorded. The coolant mass flux at any instant is then given by:

$$m_c = \frac{P_t A_t \left[\frac{2\gamma}{(\gamma-1)RT_t}\right]^{1/2} \left[1-\left(\frac{P_t}{P_2}\right)^{-\left(\frac{\gamma-1}{\gamma}\right)}\right]^{1/2}}{\left[\left(\frac{P_t}{P_2}\right)^{\frac{2}{\gamma}} \left(\frac{A_t}{A_2}\right)^2 - 1\right]^{1/2}} \qquad (1)$$

The model surface temperatures and pressures are measured and recorded as a function of time during a test. Having a temperature distribution as a function of time, one can evaluate the heat transfer rate. The temperature distribution is obtained as described above and is curve fitted using a numerical cubic spline curve fit (see ref. (16)). The temperature rate of change, dT/dt, is obtained from the derivative of this curve fit as a function of time, and the actual surface heat transfer rate is given by:

$$\dot{q} = \rho_m \, Cp_m \, \Delta \, \frac{dT}{dt} \qquad (2)$$

where, ρ_m is the density of the stainless steel of which the model is constructed, Cp_m is the heat capacity of the steel and, Δ is the local wall thickness. The Nusselt number is then computed as a function of time and is defined by:

$$Nu = \frac{\dot{q} R_o Pr}{(H_\infty - H_w)\mu_{s_\infty}} \qquad (3)$$

The instantaneous wall temperature is used to evaluate H_w, the Prandtl number is taken as .70, μ_{s_∞} is the freestream stagnation viscosity, and H_∞ the freestream stagnation enthalpy computed from the measured flow stagnation temperature.

As observed in figures (6) and (7) the RMS value of the sensor output exhibits a sharp change when the flow changes from laminar to transitional. The first instant at which this change occurs is defined as the transition location. By aligning the timing pulse on the RMS data with the timing pulses on the venturi pressures, P_t and P_2, and the venturi flow stagnation temperature T_t, the mass flow rate at transition is uniquely determined from equa-

tion (1).

Having determined the mass flow rate, the data can be presented in terms of the laminar injection similarity parameter, N_c, of ref. (11). This injection parameter is a function of the free stream Reynolds number, Mach number, stagnation enthalpy, the model geometry, and the total amount of injected mass. It is defined by the following relation:

$$N_c = \frac{m_c}{\mu_\infty R_o \bar{\rho}_{se} \bar{\beta}_{se} R_{e_\infty}^{1/2}} \tag{4}$$

with: $\bar{\rho}_{se} = \frac{\rho_{se}}{\rho_\infty}$

$$\bar{\beta}_{se} = \frac{d\bar{u}_e}{d\bar{s}}$$

$$\bar{u}_e = \frac{u_e}{V_\infty}$$

$$\bar{s} = s/R_o$$

Zero Angle of Attack

In reference (11) the laminar boundary layer was analyzed for the same geometry body as the current tests and provided a plot of Re_θ as a function of surface location and mass transfer rate; this figure is included here as figure (8). Tests were run at a specific free stream Reynolds number and with the film gauge at a particular surface location. The mass transfer was then varied to obtain the value of N_c required to initiate boundary layer transition. For the specific test conditions, one can obtain the transitional values of Re_θ by use of figure (8) and the value of N_c required for transition at that specific surface loca-

tion (which determines $\bar{s}$). From this information, various values of $Re_{\theta_{tr}}$ have been obtained at different surface locations and for different free stream Reynolds numbers. This data was then correlated in terms of the various parameters and is presented in figure (9); the surface location is included by utilizing the Lees[17] similarity parameter $\tilde{s}$ which is defined by:

$$\tilde{s} = Re_\infty (\mu_\infty R_o)^2 \int_o^{\bar{s}} \bar{\rho}_e \bar{u}_e \bar{\mu}_e \bar{r}^2 d\bar{s} \qquad (5)$$

where $\bar{\rho}_e = \rho_e/\rho_\infty$

$\bar{\mu}_e = \mu_e/\mu_\infty$

$\bar{r} = r/R_o$

The transition data is seen to correlate quite well for free stream Reynolds numbers varying by a factor of 15 and for surface locations varying from the vicinity of the injection region to distances which are far downstream. This data may, therefore, be used to determine the transitional behavior of boundary layers subjected to upstream mass transfer, for similar body geometries.

When the above data is cross-plotted as a function of surface location, for a constant free stream Reynolds number, the boundary layer relaminarization described in reference (11) is seen to occur. Figure (10) presents the mass transfer required to initiate transition as a function of surface distance. At a given location, values of N_c less than the transitional value produce a laminar flow while larger values of N_c correspond to either a transitional or a turbulent boundary layer. By considering a constant level of mass injection, at $Re_\infty = 0.4 \times 10^5$, one can now follow the behavior of the boundary layer as it progresses downstream over the surface of the blunt cone. For very low values of N_c the boundary layer is com-

pletely laminar, while for high mass transfer rates it is transitional or turbulent over virtually the entire surface. For intermediate values of the injection rate ($10<N_c<50$), however, a region of transitional flow is followed by a region in which the boundary layer has reverted to a laminar condition. Since the model length corresponds to a value of $\bar{s} = 50$, it was not possible to observe the expected transition to turbulence further downstream on the model. This relaminarization effect was only found to occur in a limited range of Reynolds numbers, i.e., at a lower Reynolds number (0.27×10^5) the typical behavior of a monotonically decreasing N_c with increasing distance along the body is observed. At this Reynolds number, transition was not found at the two forward film locations ($\bar{s} = 4.32$ and 9.09) even for large values of N_c (greater than 100).

Angle of Attack Results

For angles of attack ranging from 0 to 14 degrees both transition data and heat transfer data is presented at various downstream locations, for several meridian planes defined by ϕ, which is measured from the windward meridian.

The test conditions for the angle of attack data are as follows:

$M_\infty = 8.0$

$Re_\infty = 0.4 \times 10^5 \rightarrow 0.5 \times 10^5$

$\alpha = 2°, 6°, 10°$, and $14°$.

The extent of the injection region is indicated on all applicable figures ($\bar{s}_i = 0.52$).

Transition data obtained from a hot film gauge at $\bar{s} = 9.09$ is presented in terms of the mass transfer similarity parameter,

N_c, in figure (11).

This data is shown for three meridian planes: the windward plane (ϕ = 0°), the cross plane (ϕ = 90°) and an intermediate plane (ϕ = 60°). No transition data could be obtained at angles of attack larger than 6° at ϕ = 90° due to the unsteadiness of the RMS signal under these conditions. The large variation in film gauge output precluded the determination of an accurate location since a clear cut variation in signal intensity was not evident. This was also the case for values of ϕ greater than 90° even at lower angles of attack, and was probably caused by the cross flow separation that occurs in this region.

Some general conclusions may be reached concerning the data presented in figure (11). Angle of attack appears to produce a stabilizing effect on the boundary layer, at least on the windward surface ($\phi \leq 90°$). That is, at a given surface location larger mass injection is required to produce transition at angle of attack than in the axisymmetric flow condition. Conversely, for a given rate of mass transfer, transition will occur further downstream on the windward surface when the body is at an angle of attack. Moreover, these effects become more pronounced at increasing angles of attack. On the leeward surface, no transitional behavior was observable due to the large degree of unsteadiness that was present.

For the angle of attack test series, surface heat transfer rates were also measured to attempt to evaluate the feasibility of mass transfer under these conditions. The heat transfer data are presented in terms of the Nusselt number, which was defined previously, and is a function of the injected mass, the model

geometry, and the free stream Reynolds number. It is well known that for laminar flow the Nusselt number is proportional to the square root of the Reynolds number, therefore, in order to eliminate the effect of Reynolds number (at least for the laminar portions of the flow) the heat transfer data is presented in terms of the non-dimensional parameter $Nu/Re_{\infty}^{1/2}$. Therefore, in regions where the flow is laminar, the variations in the data are due to geometry, angle of attack, and mass injection effects only.

The symmetry plane heat transfer at α = 2°, 6°, 10° and 14° is presented in Figures 12 through 15 respectively. One may note that the zero injection heat transfer is an order of magnitude less on the downstream portion of the cone than at the stagnation point. Throughout the entire range of angles of attack considered in the current test program, upstream mass injection is seen to be capable of diminishing the maximum heat transfer to the cone surface by one order of magnitude. This is accomplished by reducing the stagnation point heat transfer to zero, and maintaining a relatively low Nusselt number over the spherical nose cap. As the angle of attack increases the effect of cooling decreases on the windward meridian but is enhanced on the leeward meridian. This is caused by two independent effects. Geometrically the injection region is fixed to the nose of the vehicle, therefore, at an angle of attack, the length of the injection surface as measured from the stagnation point on the windward meridian is proportionately less than on the leeward meridian. Secondly, since the flow is three dimensional the cross flow that develops carries coolant from the windward side of the cone to the leeward side.

At angle of attack, the surface film gauge used to detect boundary layer transition was only run at the $\bar{s}$ = 9.09 location. Some qualitative effects of angle of attack on transition may be obtained, however, from examination of figures (12) through (15); when the mass transfer is increased, a non-monotonically decreasing heat transfer at a given location implies that transition has occurred. This cannot accurately locate transition due to experimental scatter and also because of the behavior previously shown in figure (5). In any case, a general trend can be seen by observing the data along the windward meridian in figures (12) through (15). At 2° angle of attack, transitional flow appears in the vicinity of $\bar{s} \simeq 2.5$ at the lowest injection rate (N_c = 13.5). This is consistent with the zero angle of attack data where the same $N_{c_{tr}}$ was observed. At α = 6°, the data appears to remain laminar at $\bar{s} \simeq 2.5$ even at the highest mass transfer ate (N_c = 41.0). For N_c = 13.5 transition has apparently moved downstream to $\bar{s} \simeq 4$. Although these trends are only qualitative in nature, they are consistent with the more accurate film data shown in figure (11).

Figure (16) presents the heat transfer data measured in the 90° meridian plane. The major result that is observed is that for surface locations downstream of $\bar{s}$ = 3 there is very little effect on the heat transfer of either angle of attack or mass transfer. For the range in flow variables considered in the current test program, the $Nu/Re_\infty^{1/2}$ varied between 1.5×10^{-2} and 2.0×10^{-2} under all circumstances. For $\bar{s}<3$ the heat transfer is dependent on both angle of attack and mass transfer rate in the cross plane (ϕ = 90°).

V. Concluding Remarks

Tests have been conducted on a slender, spherically blunted cone with a porous tip utilized for mass injection into the boundary layer. Measurements were made on the impermeable surface downstream of the porous injection region. The major conclusions that were reached in this study may be summarized as follows:

(i) An accurate determination of the transition location may be obtained by using thin surface film gauges operated by a constant temperature anemometer system. Examination of the RMS signal provides the criteria by which transition can be determined.

(ii) A correlation of transition Reynolds numbers based on momentum thickness has been obtained in terms of the surface location and the mass transfer required to initiate transition. This data correlation may be utilized in the prediction of transition behavior with mass injection.

(iii) For a certain range of free stream Reynolds numbers, the effect of mass transfer was to initiate early transition, followed by a region in which relaminarization of the boundary layer occurred. In general, the presence of mass transfer had a destabilizing effect on the boundary layer which produced transition earlier than in the zero mass injection case.

(iv) Both surface heat transfer and transition data were obtained up to angles of attack greater than the half cone angle. Reasonable mass injection rates were found to effectively reduce the nose-tip heat trans-

fer to values which exist on the downstream conical surface, even at the highest angles of attack considered.

(v) On the windward meridian, the presence of non-zero angle of attack delayed boundary layer transition, even in the presence of the destabilizing mass transfer.

VI. References

1. Schuster, J.R. and Lee, T.G.: "Application of an Improved Transpiration Cooling Concept to Space Shuttle Type Vehicles". J. Spacecraft, 9, 11, November 1972.
2. Libby, Paul A.: "Numerical Analysis of Stagnation Point Flows with Massive Blowing". AIAA J., 8, 11, November 1970.
3. Nachtsheim, P.R. and Green, M.J.: "Numerical Solution of Boundary-Layer Flows with Massive Blowing". AIAA J., 9, 3, March 1971.
4. Moss, J.N.: "Radiative Viscous-Shock-Layer Solutions with Coupled Ablation Injection". AIAA J., 14, 9, September 1976.
5. Libby, P.A.: "The Homogeneous Boundary Layer at an Axisymmetric Stagnation Point with Large Rates of Injection". J. of the Aerospace Sciences, 29, 1, January 1962.
6. Cresci, R.J. and Libby, P.A.: "The Downstream Influence of Mass Transfer at the Nose of a Slender Cone". J. of the Aerospace Sciences, 29, 7, July 1962.
7. Feldhuhn, R.H.: "Heat Transfer from a Turbulent Boundary Layer on a Porous Hemisphere". Presented at Tenth Navy Symp. on Aeroballistics, Fredericksburg, Virginia, July 15-17, 1975.
8. Demetriades, A., Laderman, A.J., Von Seggern, L.: "Effect of Mass Addition on the Boundary Layer of a Hemisphere at Mach 6. J. Spacecraft, 13, 1, August 1976.
9. Kaattari, G.E.: "Effects of Mass Addition on Blunt-Body Boundary-Layer Transition and Heat Transfer". NASA Technical Paper 1139, January 1978.
10. Reda, D.C. and Raper, R.M.: "Measurements of Transition-Front Asymmetries on Large-Scale, Ablating Graphite Nosetips in Hypersonic Flight. Presented at the 17th Aerospace Sciences

Meeting, New Orleans, La., January 15-17, 1979.

11. Starkenberg, J. and Cresci, R.J.: "Boundary-Layer Transition on a Film-Cooled Slender Cone". AIAA J., 14, 4, pp. 461-467, April 1976.

12. Lin, T.C. and Rubin, S.G.: "Viscous Flow Over a Cone. Part 2. Supersonic Boundary Layer". Journal of Fluid Mechanics, 59, 3, pp. 593-620, July 1973.

13. Dougherty, N.S., Jr. and Steinle, F.W., Jr.: "Transition Reynolds Number Comparisons in Several Major Transonic Tunnels." AIAA Paper No. 74-627, July 1974.

14. Dougherty, N.S., Jr. and Fisher, D.F.: "Boundary Layer Transition on a 10 Degree Cone: Wind Tunnel/Flight Data Evaluation". AIAA Paper No. 80-0154, Jan. 1980.

15. Owen, F.K.: "Transition Experiments on a Flat Plate at Subsonic and Supersonic Speeds." AIAA J. pp. 518-523, March 1970.

16. Rubin, S.G. and Khosla, P.K.: "Polynomial Interpolation Methods for Viscous Flow Calculations". PIBAL No. 76-13, August 1976. J. Comp. Physics, 24, pp. 217-244, 1977.

17. Lees, L.: "Laminar Heat Transfer Over Blunt-Nosed Bodies at Hypersonic Flow Speeds". Jet Propulsion, Vol. 26, No. 4, April 1956.

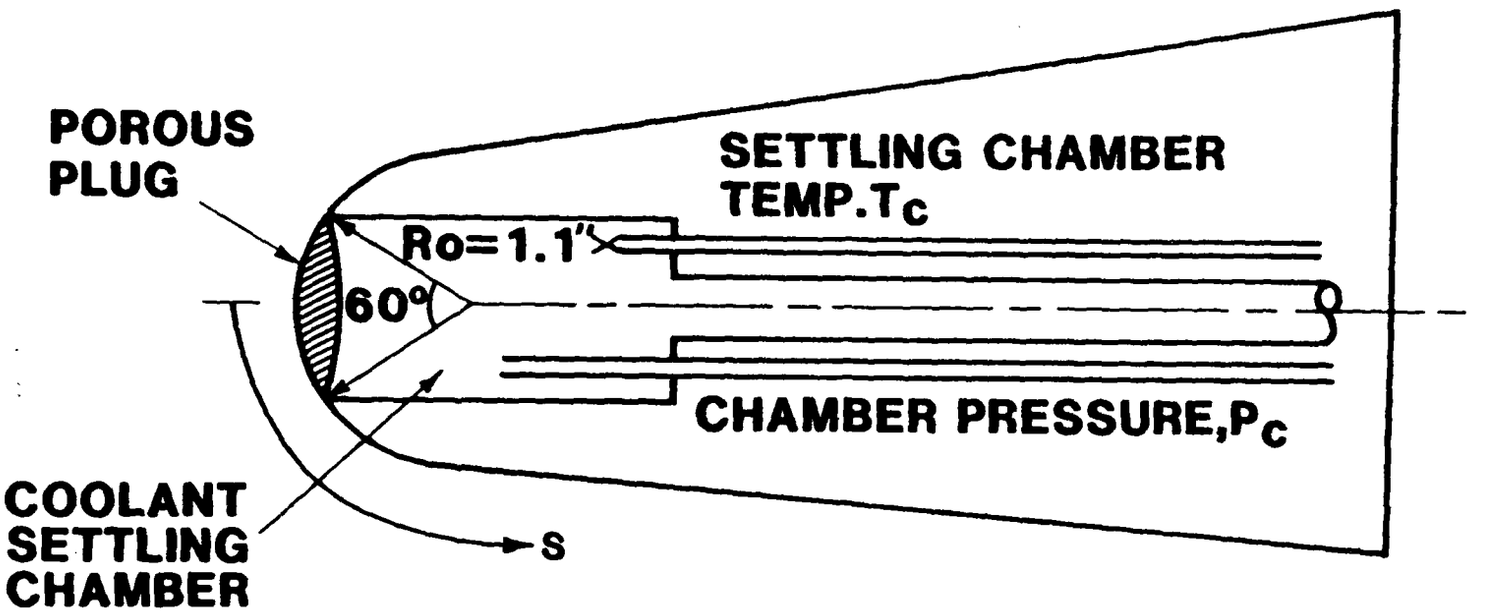

$\bar{S}$	1.36	1.82	2.27	2.95	3.64	4.32	5.45	6.96	8.47	9.09	14.66	25.0	36.8	47.0
T/C	X	X	X	X	X	X	X	X	X	X		X	X	X
FILM	X	X	X	X	X	X				X	X	X	X	X

FIG 1 MODEL SCHEMATIC

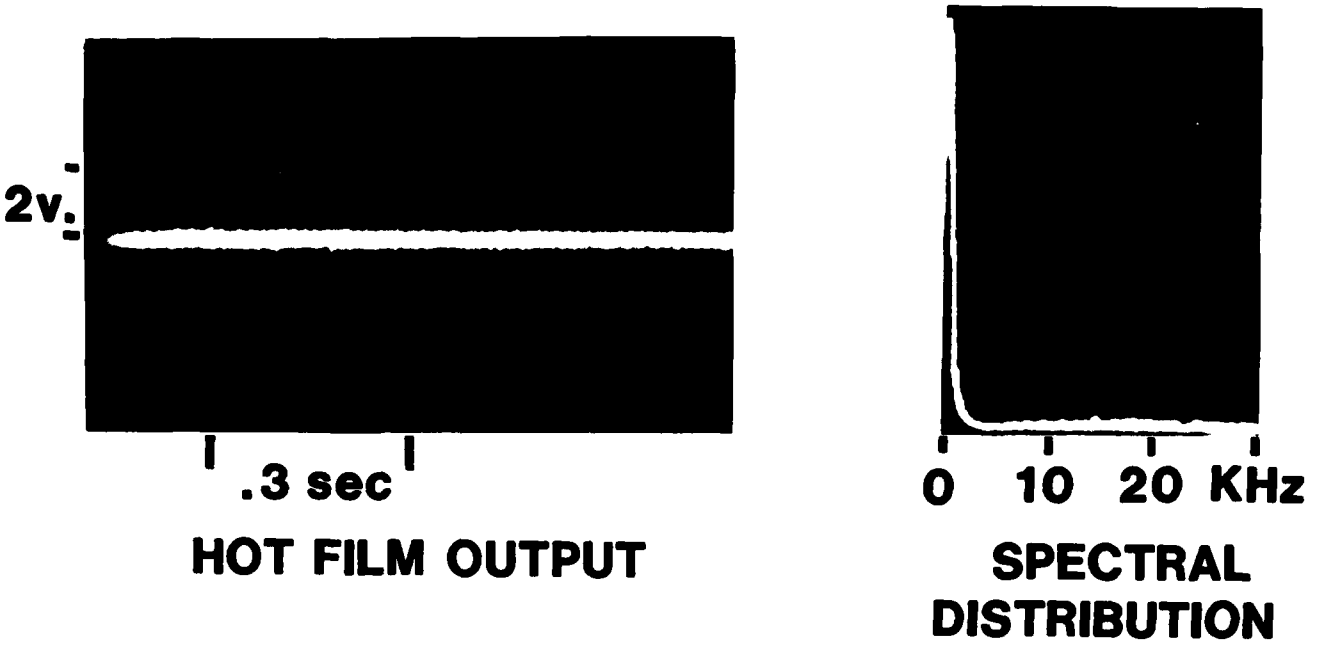

(a) Re_D = 450 (LAMINAR)

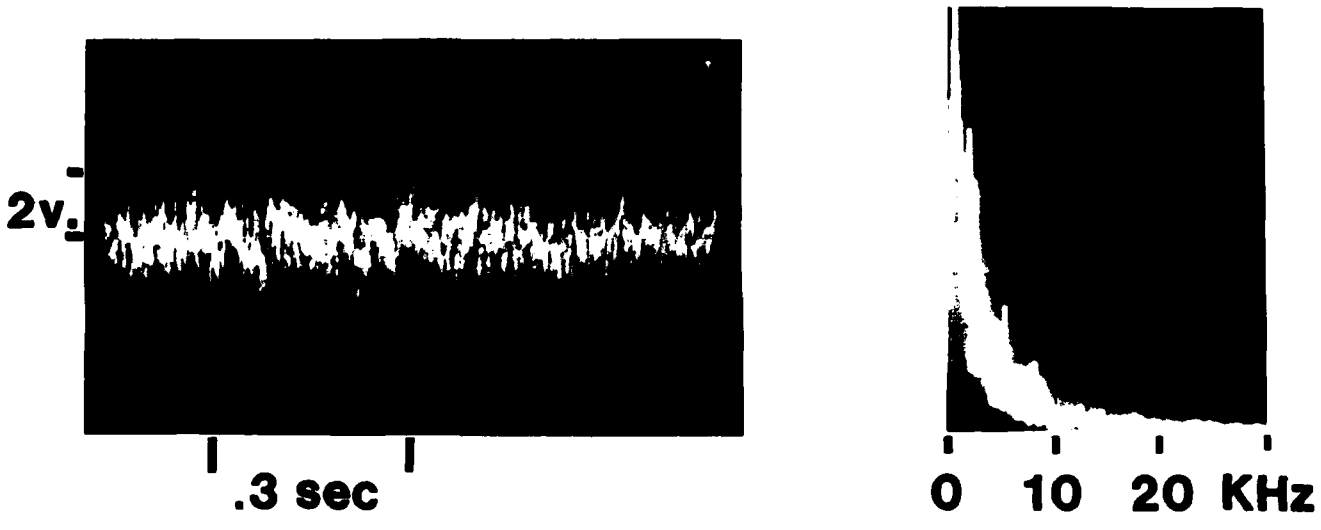

(b) Re_D = 8480 (TURBULENT)

FIG 2 FILM BEHAVIOR IN A PIPE AT LOW SPEEDS

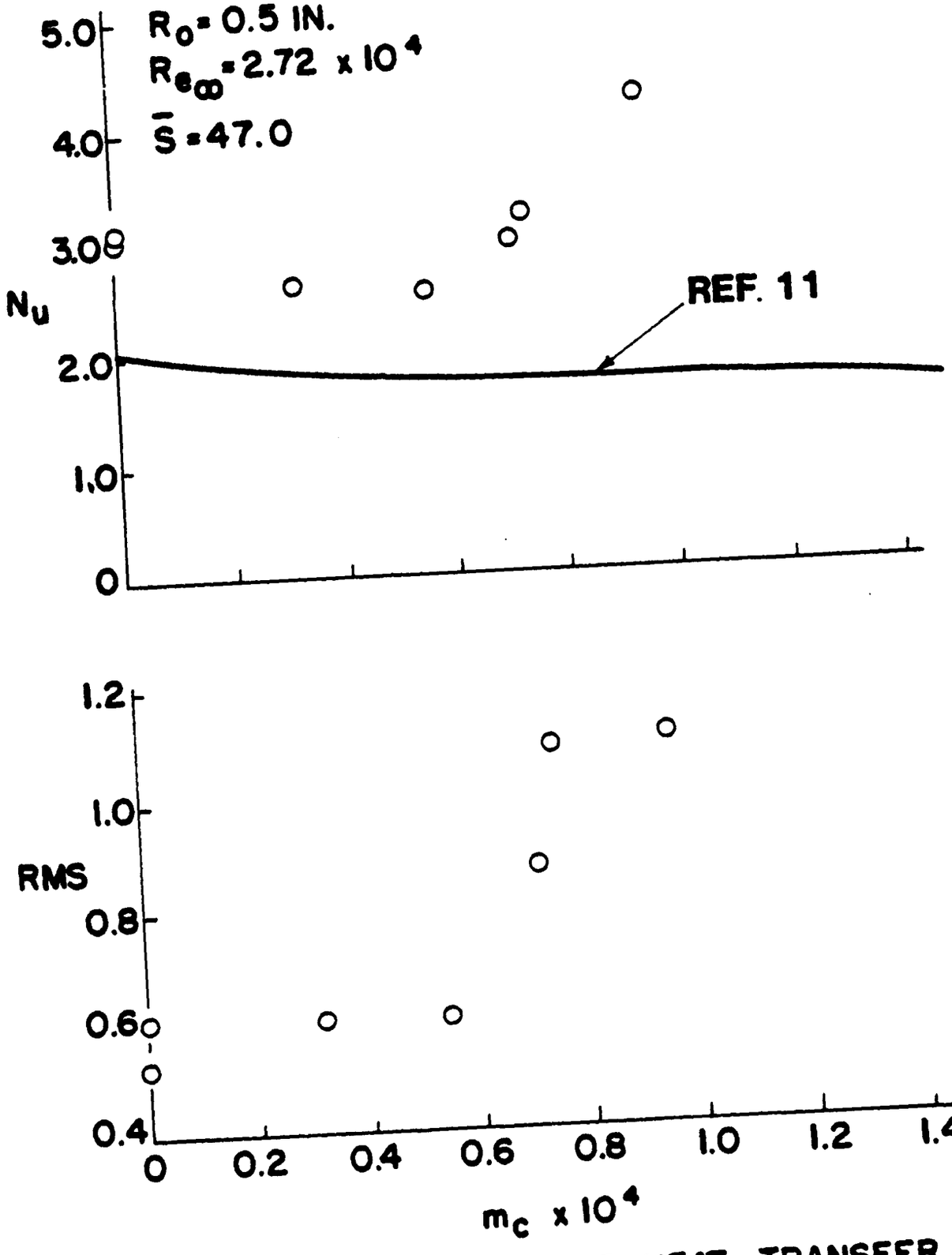

FIG 3 COMPARISON OF SURFACE HEAT TRANSFER DATA AND RMS DATA

(a) $m_c = 0$

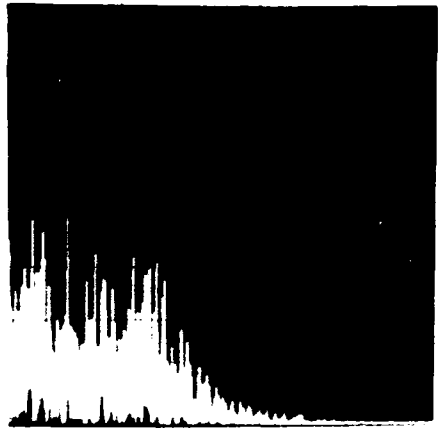

(b) 0.32×10^{-4} slugs/sec

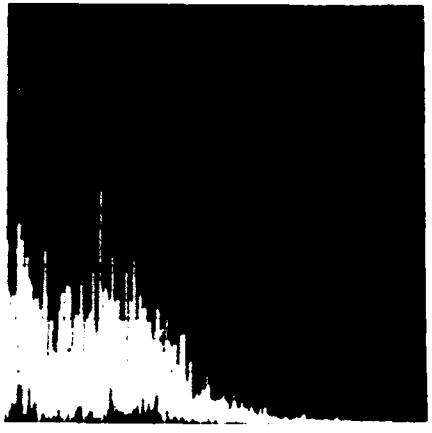

(c) 0.55×10^{-4} slugs/sec

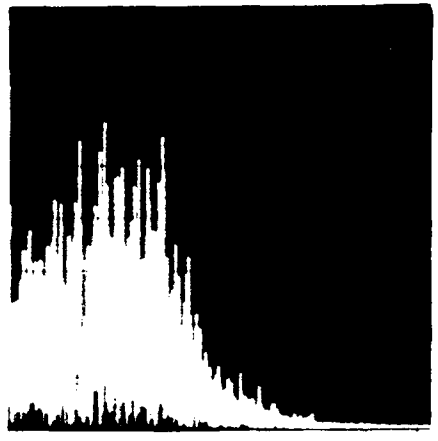

(d) 0.95×10^{-4} slugs/sec

FIG.4 SPECTRAL DISTRIBUTION OF ANEMOMETER OUTPUT
$Re_\infty = 2.72 \times 10^4$ Ro = 0.5 IN.

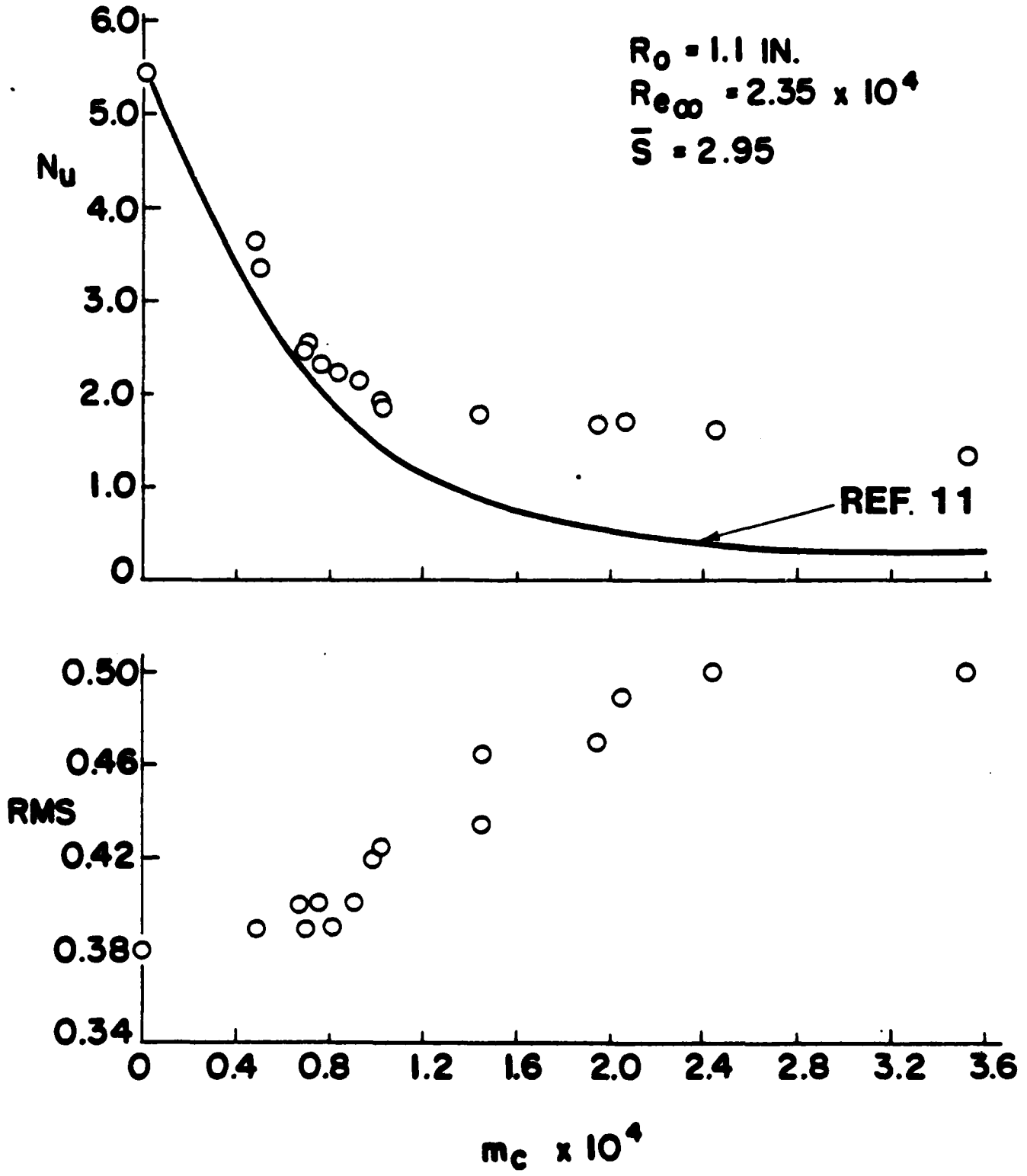

FIG 5 COMPARISON OF SURFACE HEAT TRANSFER DATA AND RMS DATA

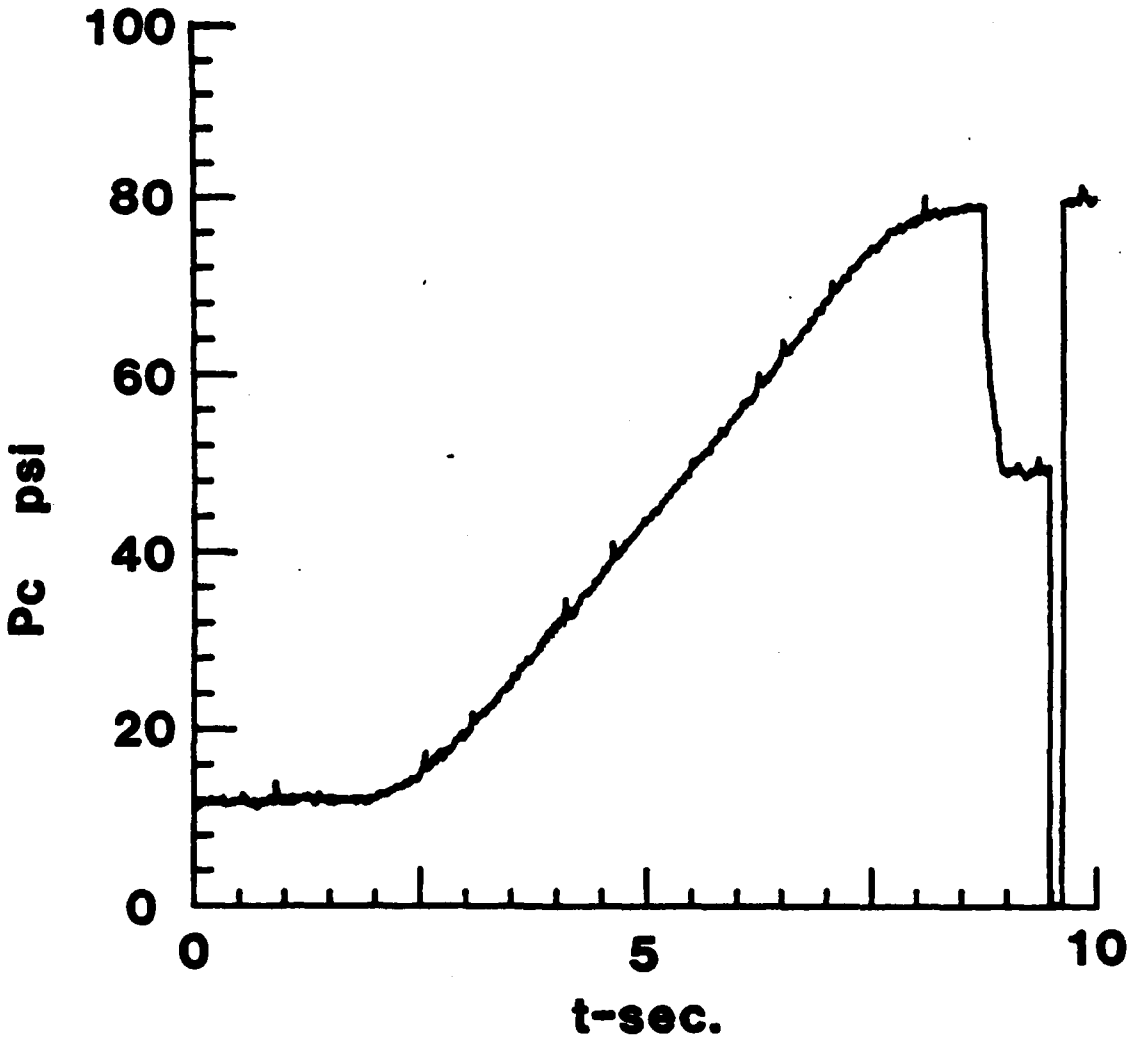

(a) CHAMBER PRESSURE

FIG 6 VARIABLE MASS FLOW $\bar{S}=36.8$

$Re_\infty=4.0\times10^4$ Ro=0.5IN. $\alpha=0°$

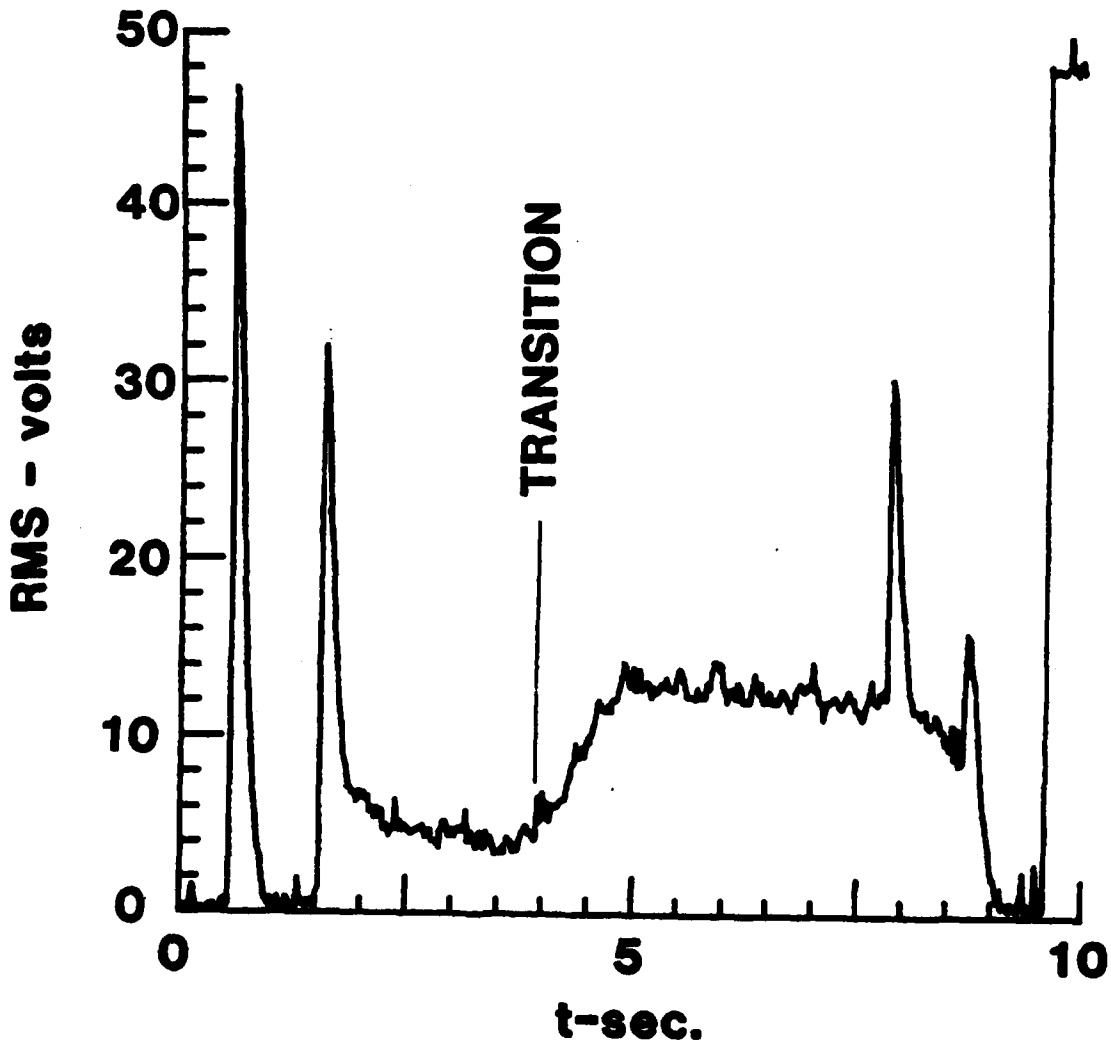

(b) RMS SIGNAL

FIG 6 VARIABLE MASS FLOW $\bar{S}$=36.8

Re_∞=4.0x10⁴ Ro=0.5IN. α =0°

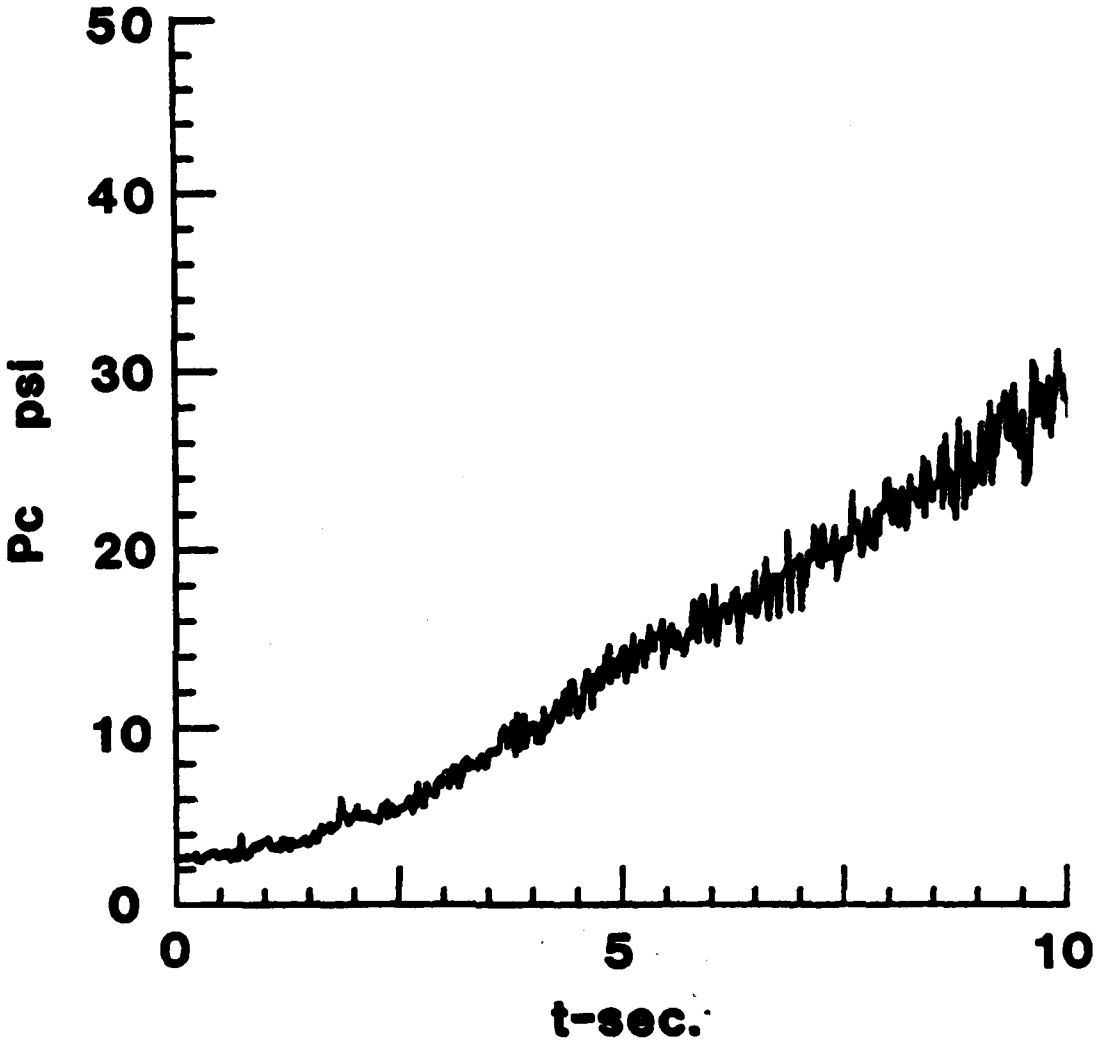

(a) CHAMBER PRESSURE

FIG 7 VARIABLE MASS FLOW $\bar{S}=9.09$

$Re_\infty=5.1\times10^4$ Ro=1.1IN. $\alpha=2°$

$\phi=60°$

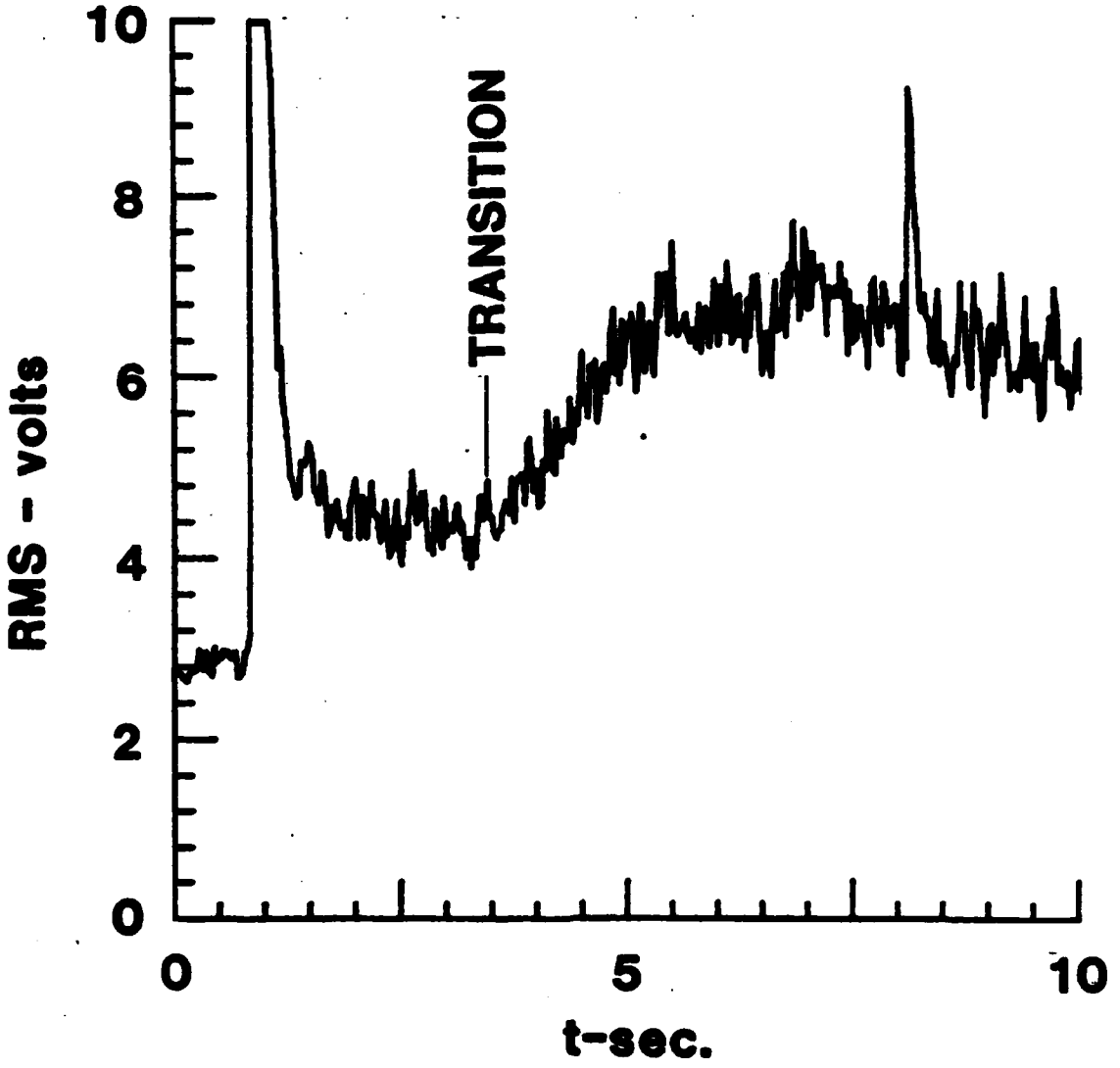

(b) RMS SIGNAL

FIG 7 VARIABLE MASS FLOW $\bar{S}$=9.09

Re_∞=5.1x10⁴ Ro=1.1IN. α =2°

ϕ=60°

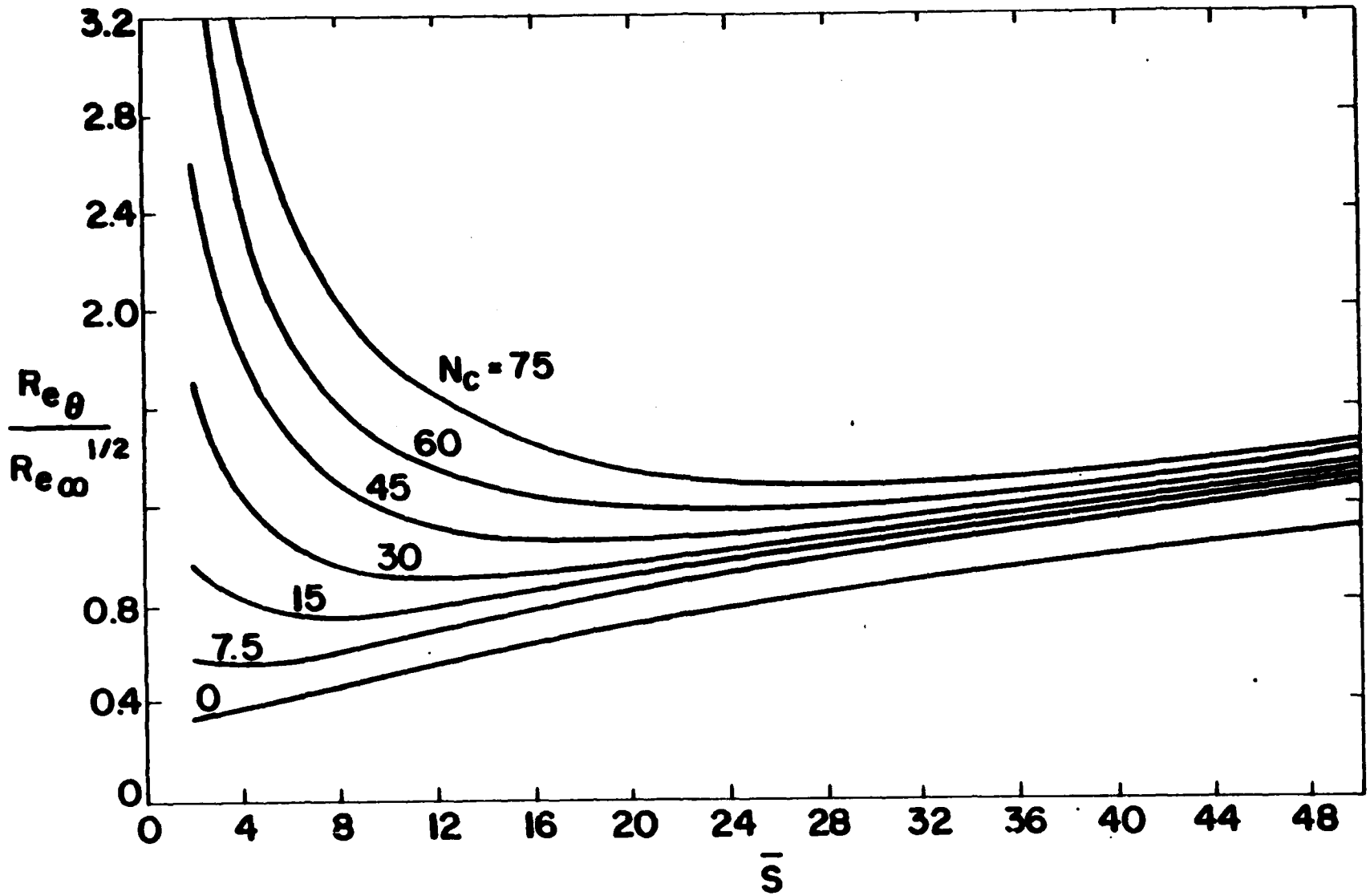

FIG 8 THEORETICAL VARIATION OF $R_{e_\theta}/R_{e_\infty}^{1/2}$ WITH DOWNSTREAM DISTANCE FOR SEVERAL VALUES OF N_c

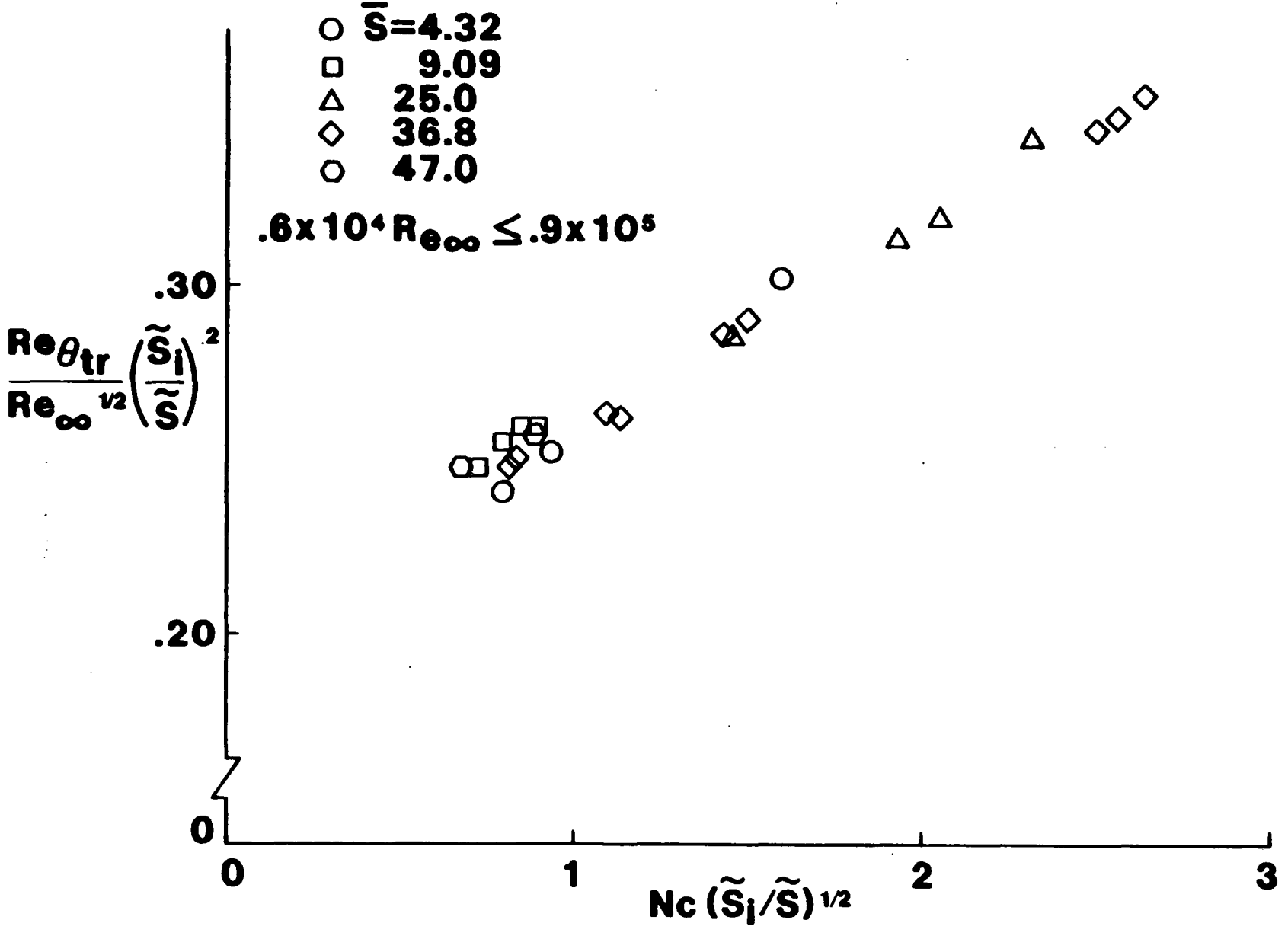

FIG 9 CORRELATION OF TRANSITIONAL Re_θ WITH MASS TRANSFER

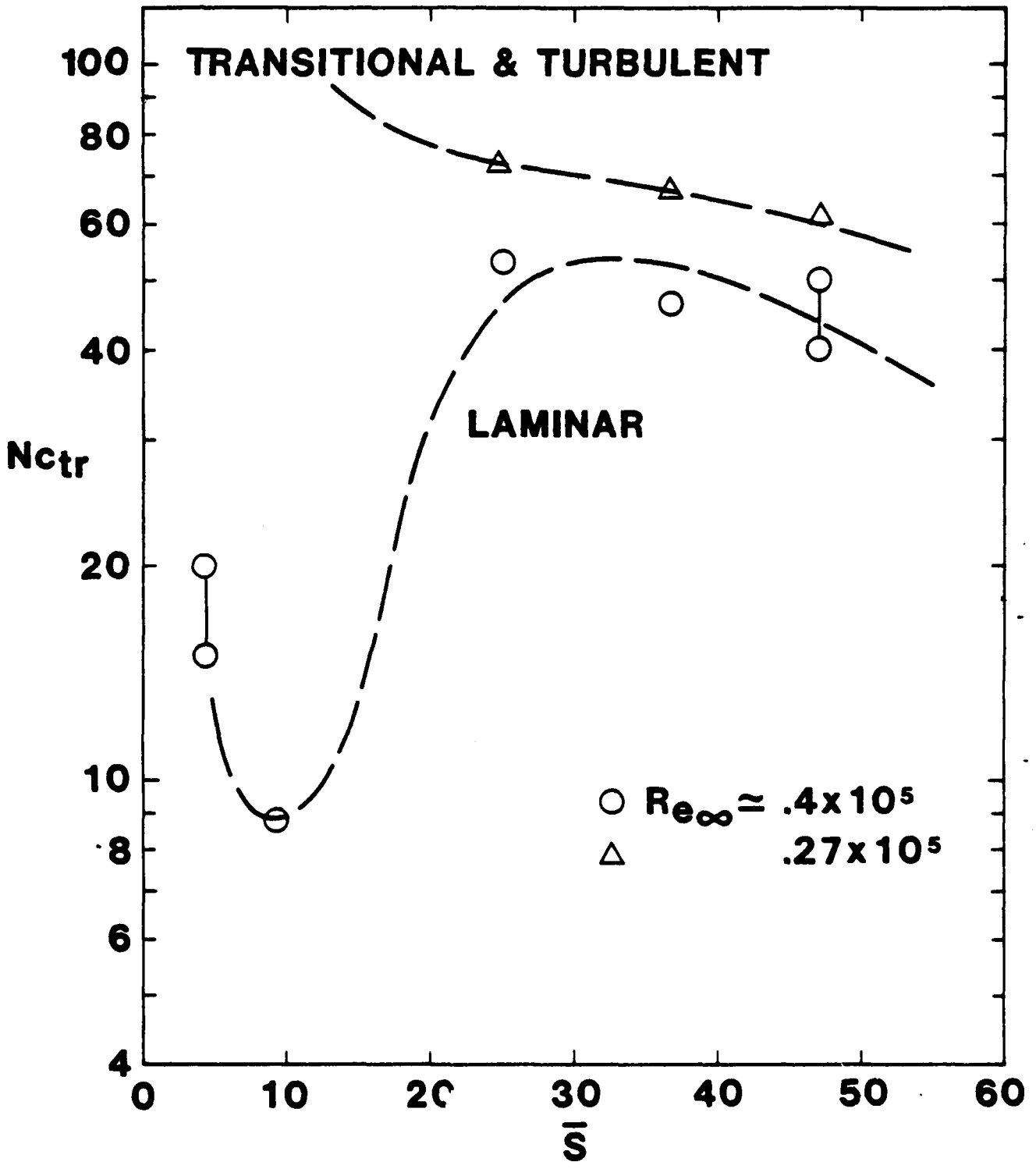

FIG 10 BOUNDARY LAYER RELAMINARIZATION

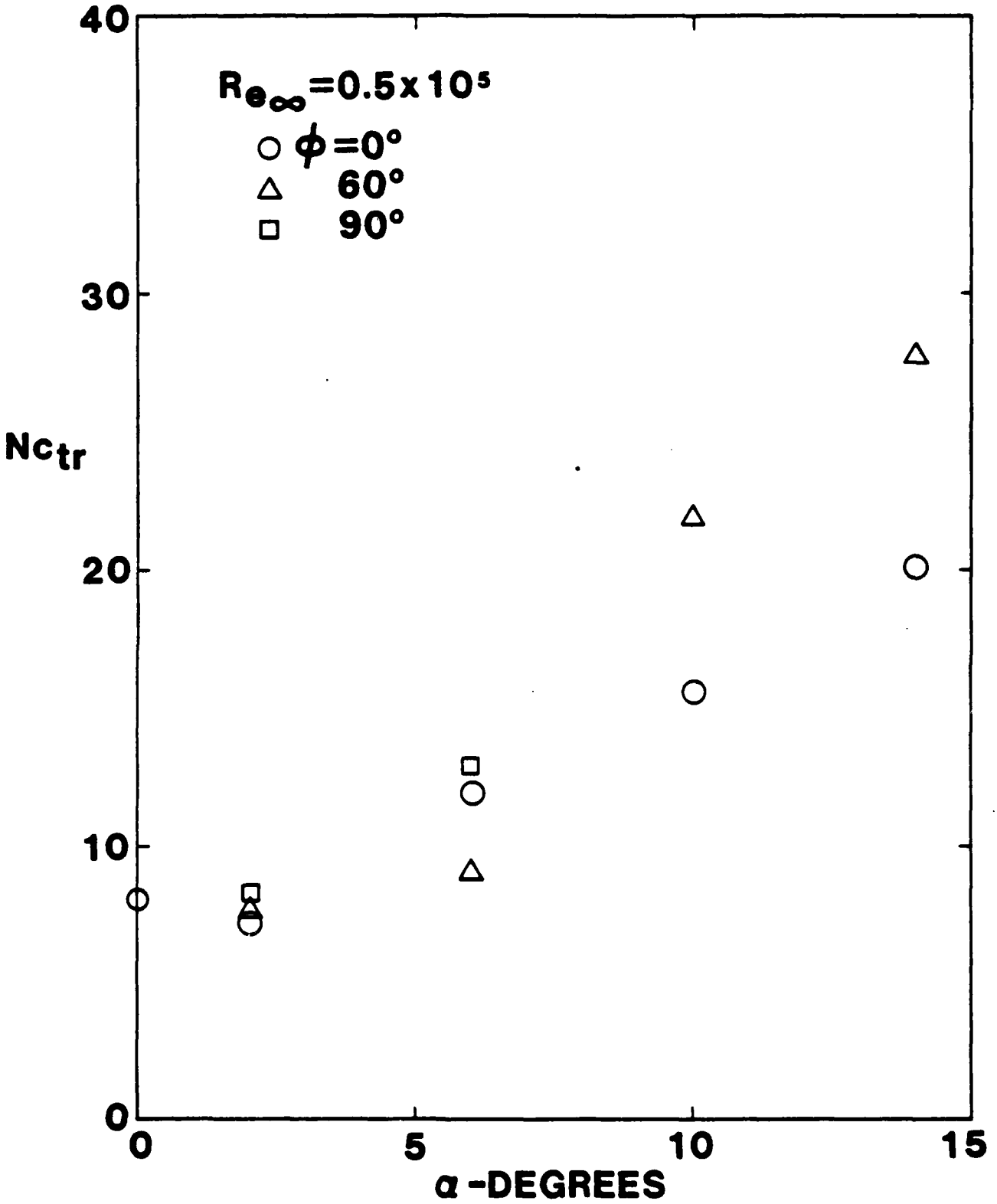

FIG 11 TRANSITIONAL BEHAVIOR at $\bar{S}$=9.09 vs. ANGLE OF ATTACK

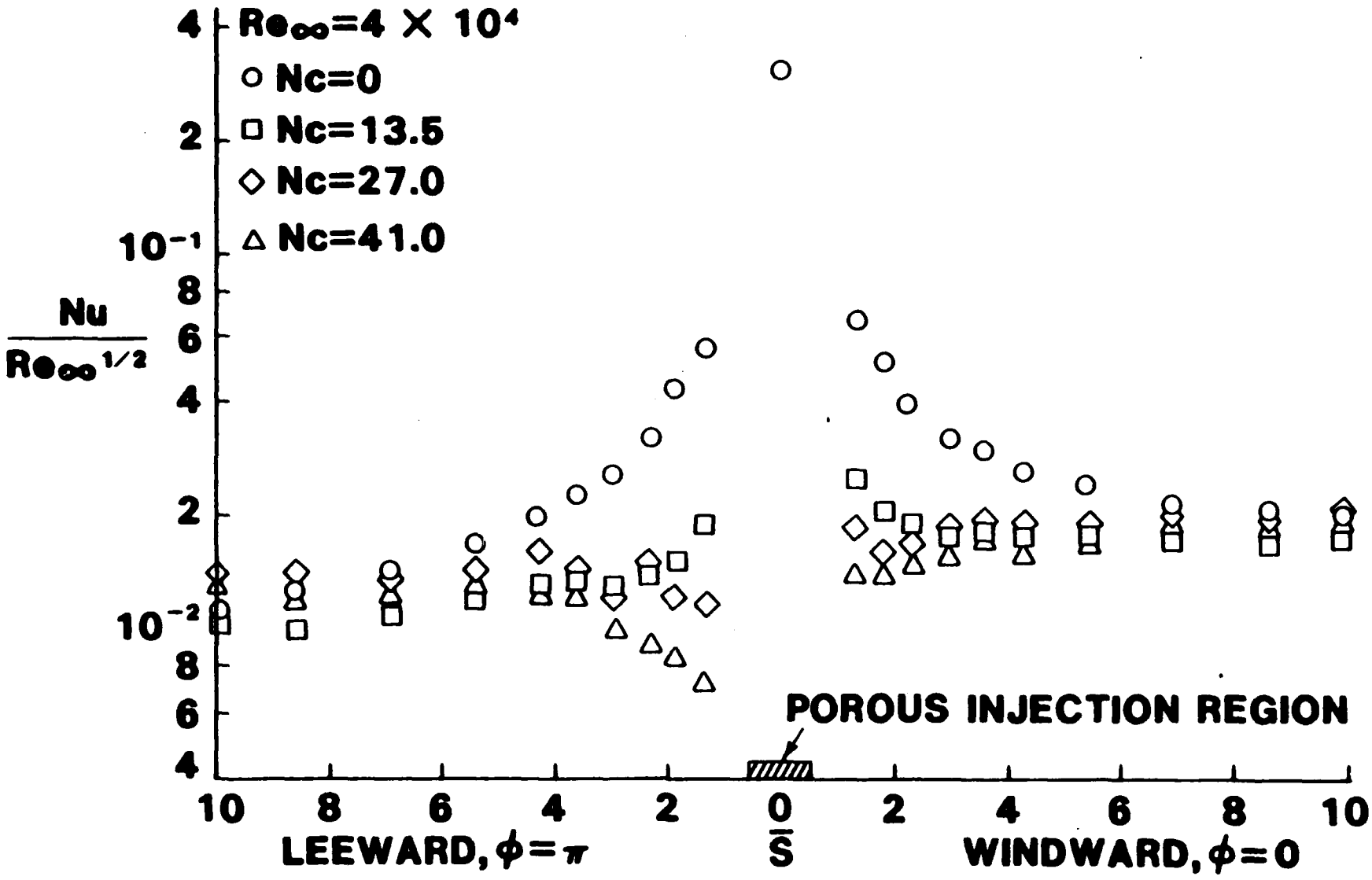

FIG 12 SYMMETRY PLANE HEAT TRANSFER $\alpha = 2°$

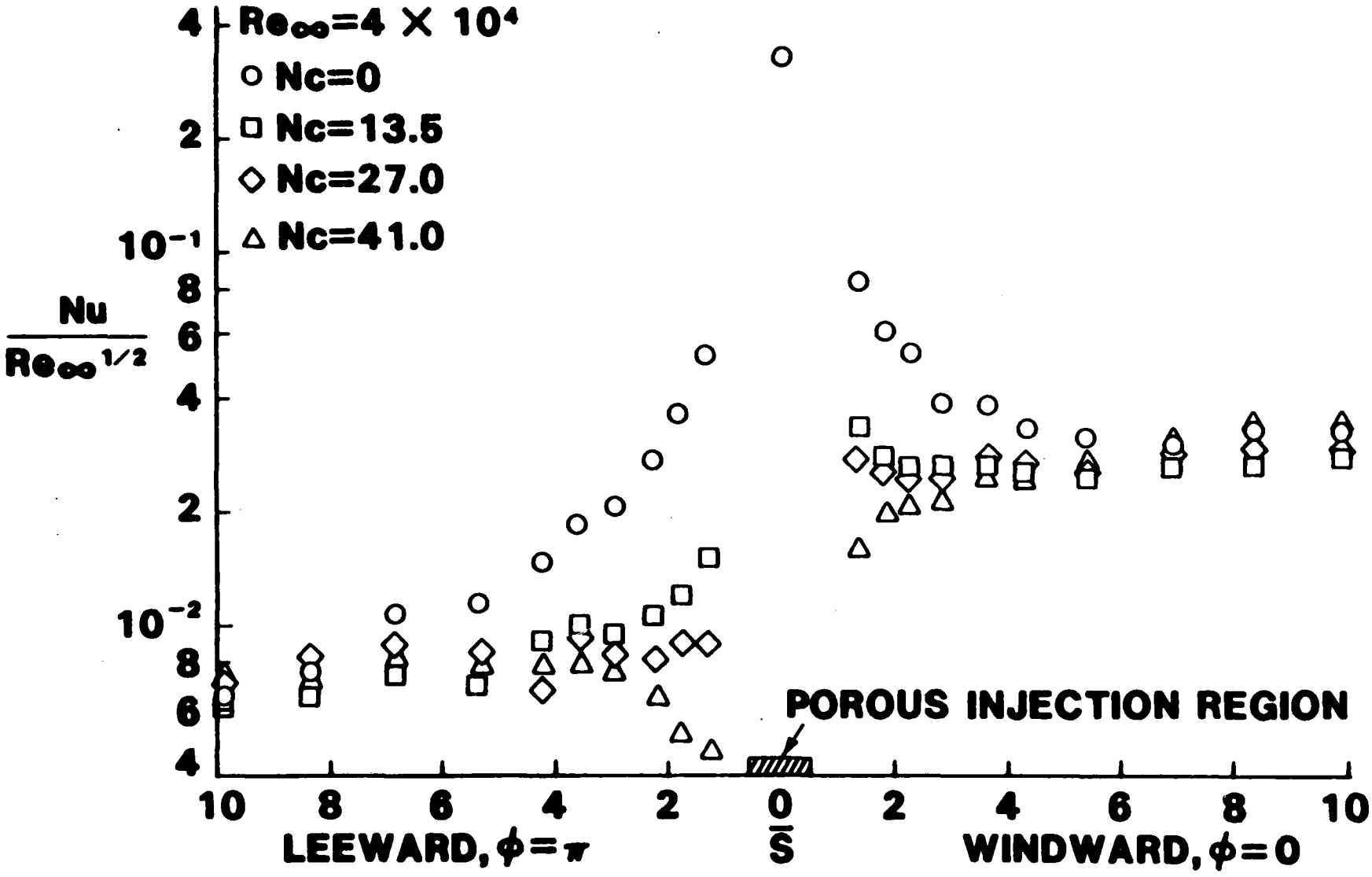

FIG 13 SYMMETRY PLANE HEAT TRANSFER $\alpha = 6°$

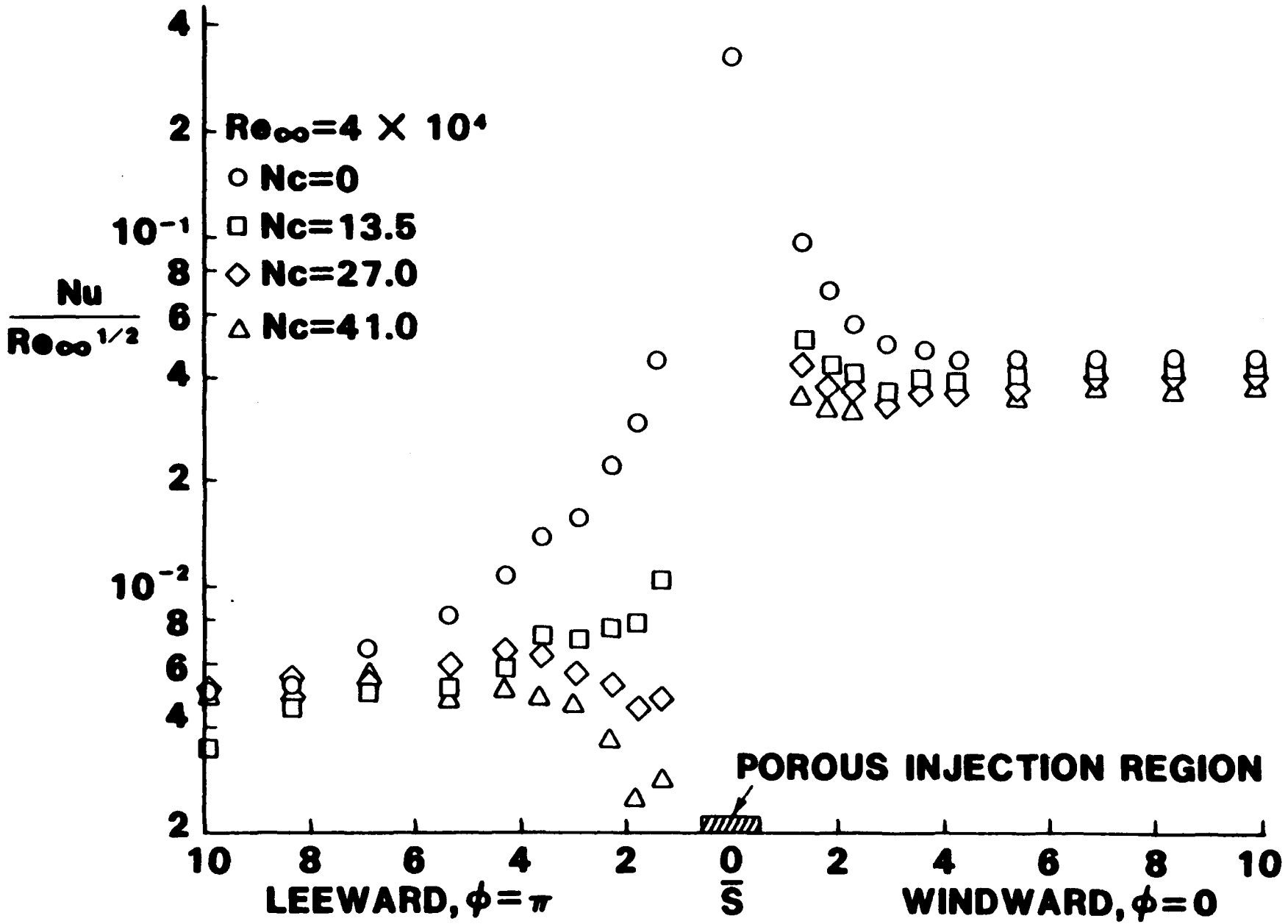

FIG 14 SYMMETRY PLANE HEAT TRANSFER $\alpha = 10°$

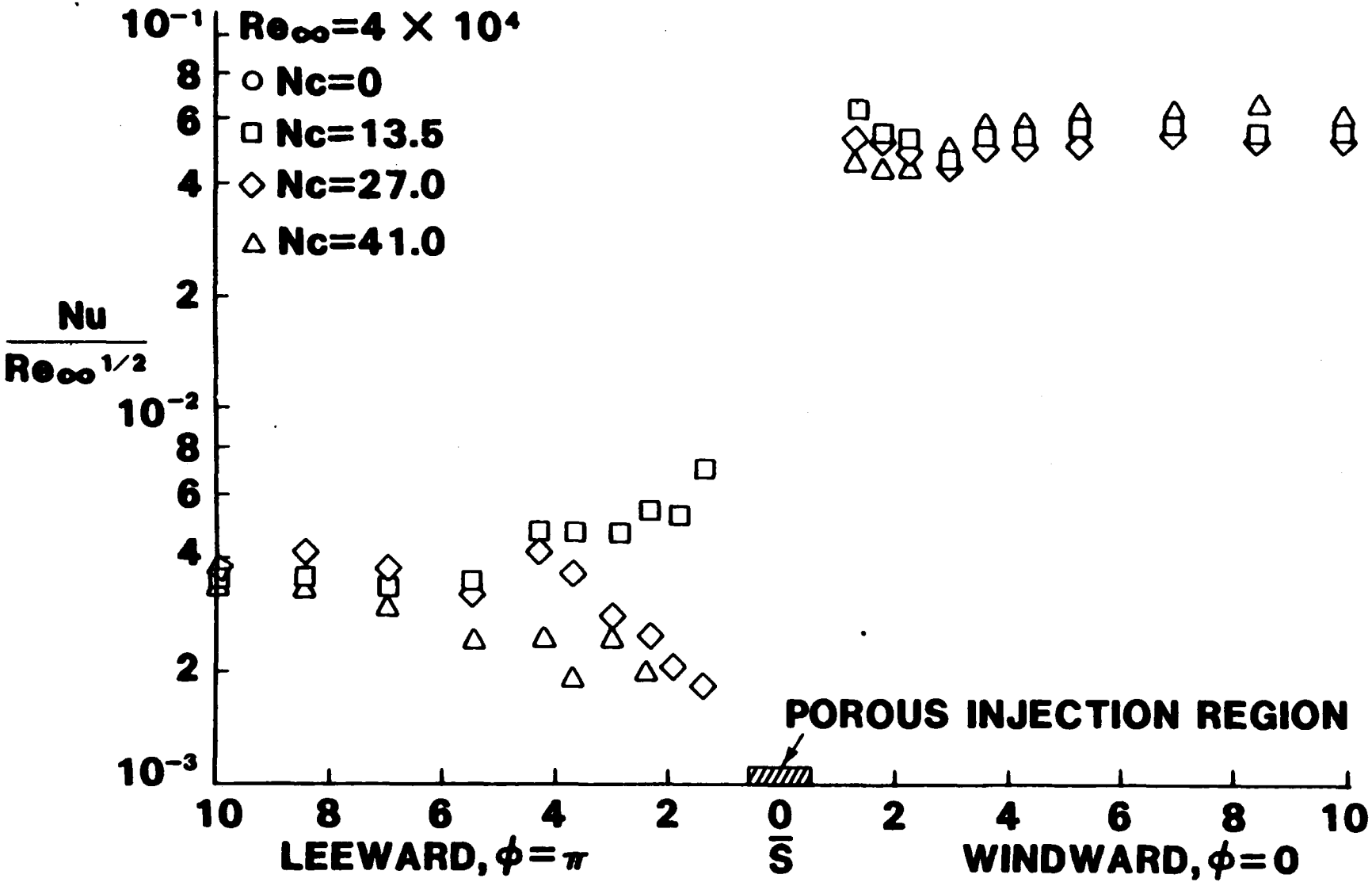

FIG 15 SYMMETRY PLANE HEAT TRANSFER $\alpha = 14°$

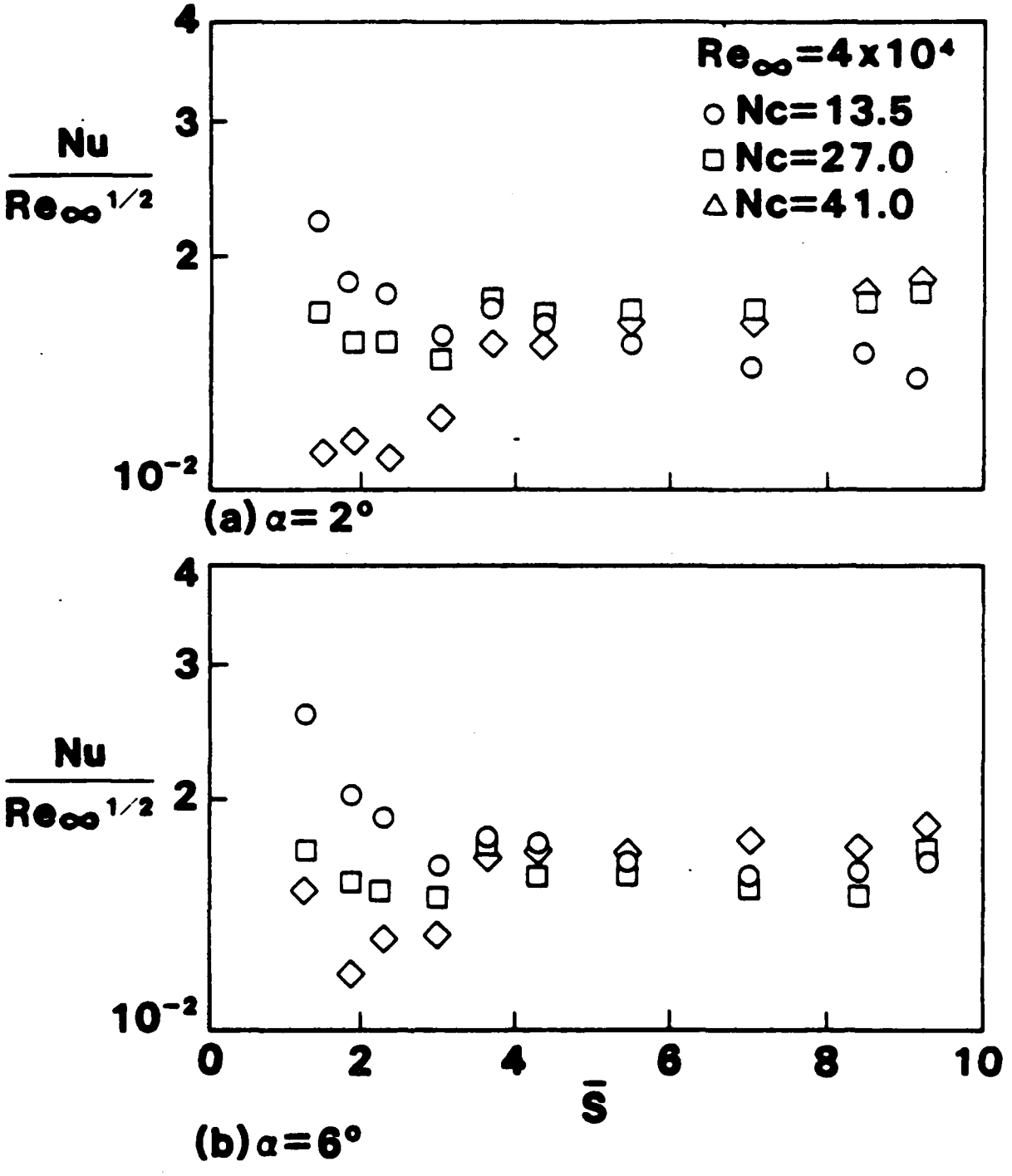

FIG 16 HEAT TRANSFER $\phi = 90°$

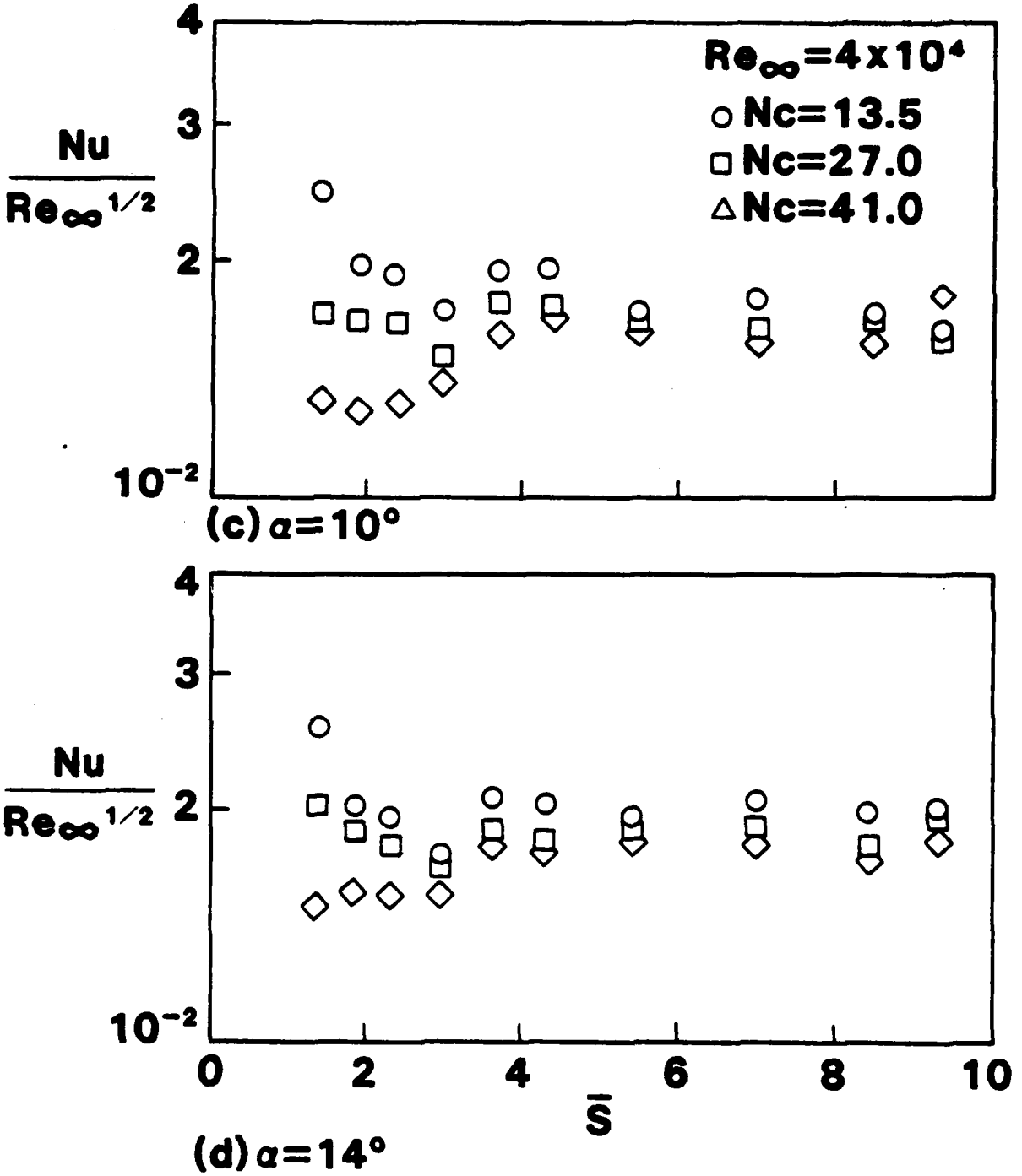

FIG 16 HEAT TRANSFER $\phi = 90°$

END

FILMED

1-83

DTIC